Structure of Triblock Copolymers of Ethylene Oxide and Propylene Oxide at the Air/Water Interface Determined by Neutron Reflection

J. B. Vieira, Z. X. Li, and R. K. Thomas*

Physical Chemistry Laboratory, South Parks Road, Oxford, OX1 3QZ, United Kingdom

J. Penfold

ISIS, CLRC, Chilton, Didcot, Oxfordshire, OX11 0QX, United Kingdom

Received: October 17, 2001; In Final Form: July 22, 2002

Neutron reflection has been used to investigate the structure of adsorbed layers of two triblock copolymers with approximate formulas $E_{23}P_{52}E_{23}$ and $E_9P_{22}E_9$, where E is ethylene oxide and P is propylene oxide. Measurements were made at the air/water interface at the critical micelle concentration and at two much lower concentrations, and at temperatures of 25 °C and 35 °C. Isotopic labeling was used to improve the resolution of the experiment. In general, the adsorbed layer can be described in terms of a minimum of four uniform sublayers. The outermost layer is always a water-free layer containing only propylene oxide (PO) residues. The ethylene oxide (EO) residues form a tail below this layer, which extends into the solution over a distance slightly shorter than the fully extended length. Depending upon the conditions, some PO is also mixed in with this tail region. For example, at the lower surface concentrations, the segment density of the (PO) decays rapidly and there is a relatively small proportion of PO immersed in the water but, at the highest concentrations, there is a much larger amount of PO in the aqueous/EO region, and this extends some way into the solution. At the higher temperature, there is little PO in the aqueous region of the layer, but there is significant mixing of PO with EO in a sublayer just below the main PO layer out of the water. The smaller molecular weight polymer gives a much more disordered structure with greater mixing of all three components. The disorder in these adsorbed layers is higher than that previously suggested for the micellar structure. Comparison of the layer structure at the air/water interface with that in micelles indicates either that there is a significant difference in the extent of mixing of the PO and EO between the two situations or that the published small-angle scattering data can be reinterpreted in terms of a micellar structure where the PO/EO mixing is more in accord with that observed at the air/water interface.

Introduction

There is no experimental information available about the organization of the water soluble triblock copolymers, poly(ethylene oxide-*b*-propylene oxide-*b*-ethylene oxide) (EPE) adsorbed at the air/water interface. Any arguments about how such molecules are oriented within the monolayer have been based on indirect arguments from surface tension measurements and correlations with studies of the configuration of the homopolymer poly(ethylene oxide) at the air/water interface. For example, Alexandridis et al.[1] suggested that at concentrations below a first inflection in the surface tension curve, these tri-block copolymer molecules adsorb at the air−water interface as an inverted U with the EO chains oriented similarly to PEO homopolymers at air/water interface. Above this break (typically at a bulk concentration of about 10^{-3} *w*/*v*%), when the interface is fully covered with copolymer, Alexandridis et al. suggested that a change in configuration takes place and that the copolymer layer becomes more compact with water molecules being excluded from the monolayer and the EO segments either extending into the aqueous solution or folding around the PPO chain. In a previous paper, we have shown that the more direct measurements of surface coverage possible with neutron reflection suggest a different picture. In particular, at concentrations varying through the first breakpoint, the neutron surface excess hardly changes with concentration, suggesting that in fact the monolayer is complete and undergoes no change in this concentration range.[2] At much higher concentrations, however, changes in the surface coverage do occur as the concentration approaches the critical micelle concentration (CMC) and these are accompanied by increases in the thickness of the layer. In the present paper, we extend the neutron reflectivity measurements to study the configuration of EPE copolymers adsorbed at the air/water interface. The effects of bulk concentration, molecular weight, and temperature on the organization of the monolayer have also been examined.

TABLE 1: Characteristics of the EPE Copolymers

formula	M_n	%EO	M_w/M_n
$E_{23}P_{52}E_{23}$	4900	41	1.03
$dE_{23}P_{52}dE_{23}$	5000	42	1.03
$E_9P_{22}E_9$	2000	40	1.04
$dE_9P_{22}dE_9$	2000	42	1.03

Experimental Details

The preparation and characterization of the polymers has been fully described in the previous paper and their characteristics are given in Table 1.

The neutron reflection measurements were made on the white beam reflectometer SURF based on the ISIS pulsed neutron

* To whom correspondence should be addressed.

10.1021/jp013851h CCC: $22.00
Published on Web 09/14/2002

source at Rutherford−Appleton Laboratory, Didcot, UK, and followed procedures that have been previously described.[3] The measurements were made at fixed incident angles of 0.8° and 1.5°. The reflectivity profiles obtained at the two angles were combined into a single reflectivity profile and calibrated with respect to D_2O. Flat backgrounds measured at high momentum transfer were subtracted for all measurements before the fitting of any models. Reflectivities are plotted against momentum transfer, κ, defined by

$$\kappa = \frac{4\pi \sin\theta}{\lambda} \tag{1}$$

where 2θ is the scattering angle and λ is the wavelength of the neutrons.

The solutions of copolymers were contained in Teflon troughs mounted on an antivibration bench and measurements were made at 25 °C and 35 °C. High purity water (Elgastat UHQ) was used for all the measurements, and all the glassware and Teflon troughs were cleaned using alkaline detergent (Decon 90) followed by rinsing with ultrapure water.

Results

The simplest neutron reflectivity profile both to understand and interpret is that from the partially deuterated polymer in null reflecting water (NRW). This can usually be fitted with a one or at most two uniform layer model and leads directly to a mean thickness of the layer and the surface excess. We have already described the application of such a model to the neutron reflectivity data in the previous paper.[2] Here, we combine these measurements with measurements of the reflectivity from the same partially deuterated polymer in D_2O and of the matched fully hydrogenated polymer in D_2O. Before presenting the details of the analysis it is useful to give a qualitative description of what information the three contrasts can give.

To a first approximation, the reflectivity of the fully hydrogenated polymer in D_2O gives the depth of water perturbed by the presence of the polymer. This is because the scattering length density of the polymer is small and the reflectivity therefore depends only on the surface normal profile of the depleted D_2O layer. Easily determined quantities are the displaced volume fraction of D_2O and the thickness of the displaced layer. In practice, at the thicknesses of 50 Å or so observed for this system the resolution of the experiment is sufficient to distinguish some of the details of the shape of the displaced D_2O profile. The displaced D_2O profile can then be directly related to the polymer volume fraction profile using the assumption of space filling. However, because there is little difference in the scattering length densities of ethylene and propylene oxides no distinction between them is possible on the basis of this profile alone. Such information has to be obtained from the reflectivity of the partially deuterated polymer in D_2O. In the present case, it is the EO part of the polymer that is deuterated. To a first approximation, the PPO fragment is then invisible and the PEO fragment will have a scattering length density rather similar to D_2O. Thus, if D_2O were displaced from the surface region only by the deuterated EO fragments and if all the EO fragments were immersed in the D_2O, the reflectivity would be similar to that from D_2O on its own. Combining the measurements from the two isotopic compositions would then clearly identify this element of the structure if it were present. The actual details can be further refined by combining the information from the two D_2O profiles with the NRW measurements. The latter give an overall thickness of the deuterated part of the layer, irrespective of where the water is in the layer. For all three measurements, the thickness of the layer is large enough that the resolution with which the structure can be determined is significantly better than for a small molecule surfactant. The general fitting strategy is to fit a single structural model to the three contrasts using the minimum number of layers required for a satisfactory fit.

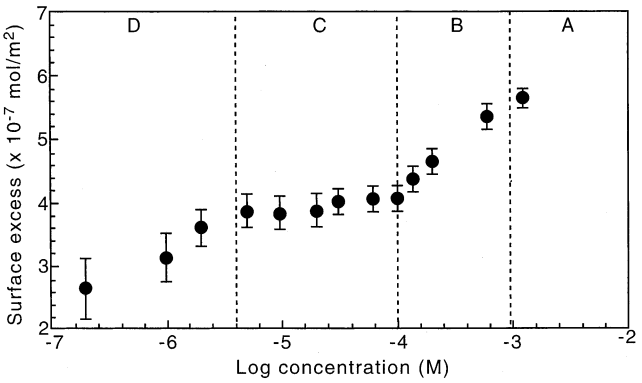

Figure 1. Adsorption isotherm of $E_{23}P_{52}E_{23}$ at the air−solution interface at 25 °C determined by neutron reflection.

We start by considering the structure of the $E_{23}P_{52}E_{23}$ monolayer. We have shown in the previous paper that the adsorption isotherm, reproduced in Figure 1, indicates that there are structural transitions within the layer. Four different sections of the isotherm were identified in which the monolayer structure and the adsorption behavior of the copolymers appear to change with bulk concentration. Section D of the isotherm is associated with a region where the surface coverage is dominated by depletion of the copolymer from the solution and by nonequilibrium effects at the surface. In section C, the surface excess has the relatively constant value characteristic of a saturated monolayer. In this region, the surface tension varies linearly with ln *c*. Section B is characterized by quite a steep increase in the surface coverage without any associated change in the monolayer thickness. This change has to be associated with a change of the arrangement of the copolymer molecules within the monolayer. Section A is where the bulk solution is micellar and in this region adsorption should again reach a plateau.

To explore these changes, the reflectivities of the three isotopic compositions, dEPdE in NRW, dEPdE in D_2O, and hEPhE in D_2O, were measured at three different concentrations at 25 °C. The concentrations were 1.2×10^{-3} M, 2.0×10^{-5} M and 2.0×10^{-6} M, which fall within sections A, C, and D, respectively. We chose to fit the data by starting with a model structure in which the uppermost layer comprises only PO groups and air, whereas the remaining layers are regarded as completely immersed in the water, that is, the volume fractions of PO, EO, and water add up to unity in all layers except the top one. A further important constraint on the model is that the known stoichiometry of the polymer must be satisfied. Although the basic scattering parameters are all well established from other measurements (Table 2), it is worth noting that the least reliable ones are the volumes of the two polymer segments, which have been estimated from the densities of the bulk materials. Such an estimate takes no account of volume changes on mixing, and these values probably have an uncertainty of about 5%, which will feed through to create comparable errors in the structural analysis. There is also, of course, an uncertainty in the stoichiometry in that the mean stoichiometry may not be an accurate reflection of the stoichiometry of those species that are most strongly adsorbed at the interface. However, these are likely to be relatively minor inaccuracies compared with the overall resolution of the experiment. For the highest concentra-

TABLE 2: Scattering Properties of the Components of the Layer

species	scattering length/Å	molecular volume/Å^3	scattering length density/Å^{-2}
dEO	4.40×10^{-4} (96%D)	64.6	6.81×10^{-6}
hEO	4.14×10^{-5}	64.6	0.64×10^{-6}
hPO	3.31×10^{-5}	96.5	0.34×10^{-6}
D_2O	1.91×10^{-4}	30	6.35×10^{-6}
H_2O	-1.68×10^{-5}	30	-0.56×10^{-6}
NRW	0	30	0

tion, 1.2×10^{-3} M, a minimum number of five layers were required to give a satisfactory fit to the three profiles. The three profiles and the best fits are shown in Figure 2. For the other two concentrations, 2.0×10^{-5} M and 2.0×10^{-6} M, good fits were obtained with a model of four layers and these are shown in Figures 3 and 4, respectively.

The structural parameters derived for the three concentrations are given in Table 3 and we have presented these in a different way from our previous work. Rather than give values for the scattering length density for each of the three isotopic compositions, we have given the values of ρ corresponding to the deuterated polymer in D_2O together with the volume fraction of water in each component layer, ϕ_{water}. The composition of the layer can be obtained from

$$\rho = (1 - \phi_{water})\rho_{polymer} + \phi_{water}\rho_{water} \quad (2)$$

The actual fitting parameters are the thickness of each layer, $\rho_{polymer}$ and ϕ_{water}. The polymer composition in the layer is determined by

$$\rho_{polymer} = \phi_{PO}\rho_{PO} + (1 - \phi_{PO})\rho_{DEO}$$

where ρ_{PO} and ρ_{DEO} are given in Table 2. The use of only this value of the scattering length density makes it possible to reconstruct the whole set of fitting parameters from the table while greatly reducing the number of parameters actually tabulated. Not surprisingly, given the discussion of the qualitative effects of the different contrasts the reflectivity is not generally sensitive to the structure of the upper layer (layer 1) because of the low scattering length density from the PO groups. A more precise description of that layer would require the PO segments to be deuterated. However, the reflectivity profiles are very sensitive to the composition and thicknesses of the remaining layers and the constraint of stoichiometry defines the total amount of PO in the upper layer extremely accurately. The uncertainties lie in its its thickness and density. The five

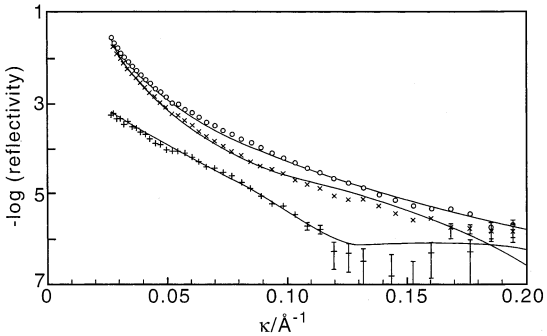

Figure 2. Neutron reflectivity profiles from the air/water surface of different isotopic compositions of 1.2×10^{-3} M $E_{23}P_{52}$ E_{23} at 25 °C. The observed profiles are shown as points, (○) dEhPdE in D_2O, (×) hEhPhE in D_2O and (+) dEhPdE in NRW. The best fits of a single structure to all three profiles, using the parameters in Table 3, are shown as continuous lines.

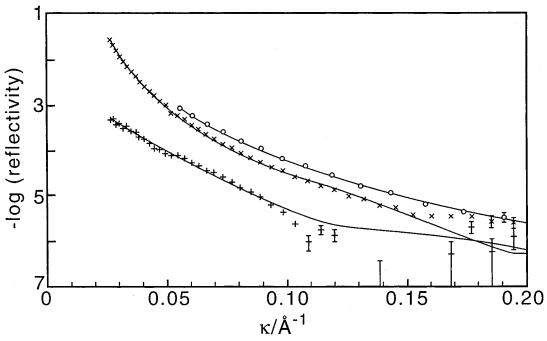

Figure 3. Neutron reflectivity profiles from the air/water surface of different isotopic compositions of 2.0×10^{-5} M $E_{23}P_{52}$ E_{23} at 25 °C. The observed profiles are shown as points, (○) dEhPdE in D_2O, (×) hEhPhE in D_2O and (+) dEhPdE in NRW. The best fits of a single structure to all three profiles, using the parameters in Table 3, are shown as continuous lines.

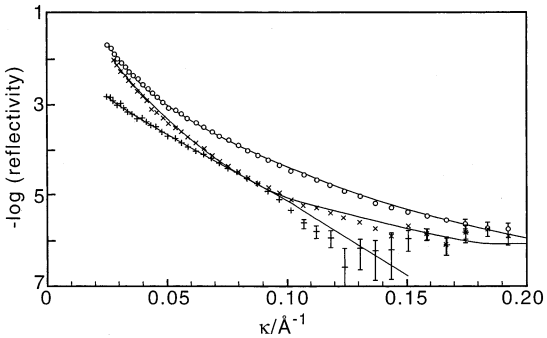

Figure 4. Neutron reflectivity profiles from the air/water surface of different isotopic compositions of 2.0×10^{-6} M $E_{23}P_{52}$ E_{23} at 25 °C. The observed profiles are shown as points, (○) dEhPdE in D_2O, (×) hEhPhE in D_2O and (+) dEhPdE in NRW. The best fits of a single structure to all three profiles, using the parameters in Table 3, are shown as continuous lines.

TABLE 3: Parameters for the Minimum Number of Layers Required to Fit the Interfacial Structure at Three Isotopic Compositions of $E_{23}P_{52}E_{23}$ in Water at 25 °C[a]

	concentration/M	1.2×10^{-3}	2.0×10^{-5}	2.0×10^{-6}
layer 1	τ_1/Å	12	11	10
	$10^6\rho$/Å^{-2}	0.3	0.3	0.3
	ϕ_{water}	0	0	0
layer 2	τ_2/Å	4	15	17
	$10^6\rho$/Å^{-2}	2.35	4.0	4.4
	ϕ_{water}	0.05	0.60	0.65
layer 3	τ_3/Å	11	29	29
	$10^6\rho$/Å^{-2}	2.7	6.0	6.1
	ϕ_{water}	0.52	0.85	0.90
layer 4	τ_4/Å	20	15	16
	$10^6\rho$/Å^{-2}	5.35	6.4	6.4
	ϕ_{water}	0.69	0.98	0.98
layer 5	τ_5/Å	25		
	$10^6\rho$/Å^{-2}	6.4		
	ϕ_{water}	0.90		

[a] ρ denotes scattering length density and τ denotes layer thickness.

(or four) layer model results in a greater overall thickness of the layer than the single layer model used to determine the surface excesses and described in the previous paper. Thus the total thickness of the five-layer model monolayer at a bulk concentration of 1.2×10^{-3} M, is 72 Å, compared with the thickness of 54 Å for the single-layer model. The discrepancy is simply that the upper layer, which consists only of PO fragments and air, makes only a small contribution to the reflectivity of the partially deuterated copolymer in NRW.

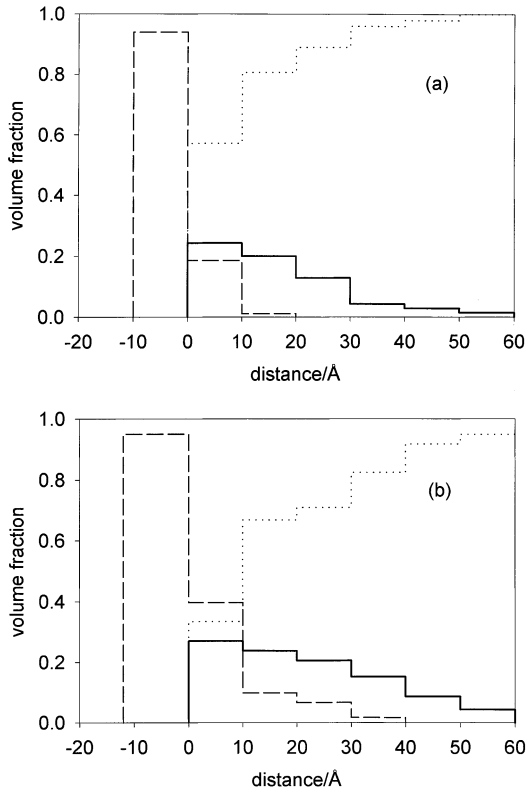

Figure 5. Volume fraction profiles of the three components PO (dashed line), EO (continuous line), and water (dotted line) at the air/water interface at 25 °C for bulk concentrations of (a) 2.0×10^{-6} M and (b) 1.2×10^{-3} M $E_{23}P_{52}E_{23}$.

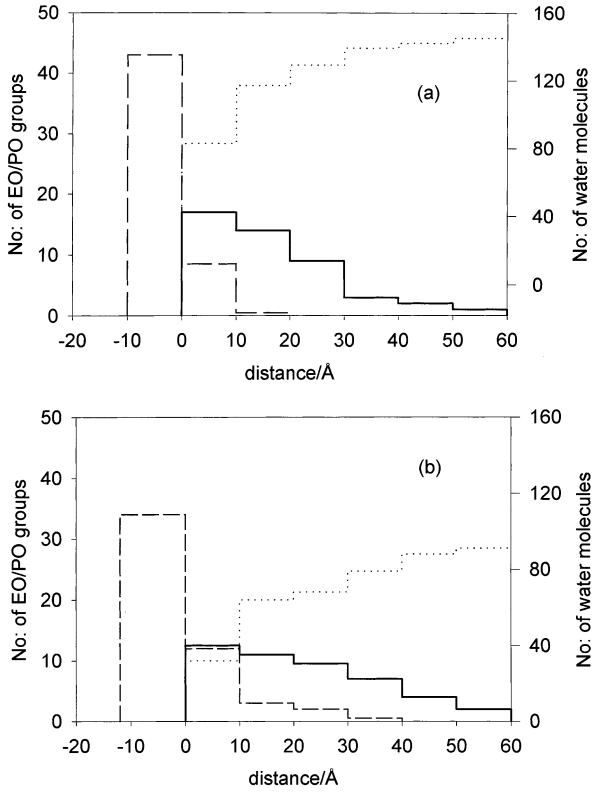

Figure 6. Profiles of the total numbers of monomer units in adsorbed layers of $E_{23}P_{52}E_{23}$ at 25 °C for bulk concentrations of (a) 2.0×10^{-6} M and (b) 1.2×10^{-3} M. (PO (dashed line), EO (continuous line) and water (dotted line)). Unlike Figure 5 the two sets of data have been normalized to the same coverage.

The uniform layer model is coarse and produces unrealistically abrupt changes in the segment distribution profile. A more realistic description of the layer would be in terms of smoother distribution functions. We therefore refitted the data using a larger number of layers but making the variation of the segment density more gradual in comparison with the minimum number of layers required to give a satisfactory fit. This gives a more realistic distribution without changing the underlying simpler model and makes it easier to compare the data with theoretical profiles. The quality of the fits to the data remains the same. That the cruder structural model is adequate to explain the data is an indication of the true resolution of the experiment, which cannot distinguish between the coarse distributions of Table 3 and those replotted in terms of smoother distributions in Figures 5 and 6 where we compare the structures at the highest and lowest concentrations in terms of volume fraction (Figure 5) and numbers of groups (Figure 6).

The volume fraction profiles of Figure 5 show that the thickness of the upper layer containing only PO segments increases only slightly over the range of copolymer concentration studied, although the number of segments adsorbed has increased by about 50%. The additional PO segments are mainly accommodated in the layers below the top layer and are evidently more extended at the higher concentration. The marked change in shape of the PO profile is emphasized more in Figure 6 where the profiles are normalized to the same coverage. The ratio of the number of PO groups out of water to the total number of PO groups changes from 0.83 at 2×10^{-6} M to 0.65 at 1.2×10^{-3} M. The change in shape of the PO distribution causes greater exclusion of water from the layers nearest the uppermost layer. The shape of the EO segment distribution also changes between the two concentrations, falling off rapidly at about 30 Å from the surface at 2×10^{-6} M. At the higher concentration, the EO distribution starts to become more like that of a polymer brush. The expected fully extended length for a PEO chain containing 23 EO segments is 74 Å, taking the length of an individual ethylene segment to be approximately 3.2 Å. Thus, the thickness of the EO layer suggests that the EO chains would be fairly fully extended if one end was anchored at the surface ($z \leq 0$). However, the presence of a significant fraction of PO in the aqueous phase suggests that the ends of the EO chains may already be significantly below the surface and hence there must be some coiling of the PEO. We discuss this further below. It is worth noting that the EO groups are always associated with water even when mixed with PO segments. Table 3 shows that the changes between the adsorbed layer at 2×10^{-6} M and 2×10^{-5} M are insignificant and therefore only the sharp increase in adsorbed amount between sections B and A of the isotherm of Figure 1 is associated with a marked change in the structure. The explanation given by Alexandridis et al. that the low-concentration break is a result of rearrangement of the copolymer molecules on the surface, therefore does not apply to our samples, although it could be a feature associated with the lower purity of the commercial samples they used.

The properties of aqueous solutions of EPE copolymers are known to be very sensitive to temperature and in this respect this class of polymeric surfactants is quite different from the small molecule C_nE_m surfactants. The change of coverage between 25 °C and 35 °C was discussed in the previous paper. Below the CMC, there is a significant increase in the total amount of adsorbed EPE copolymer with increase of temperature, without significant change to the monolayer thickness. This can be interpreted in terms of reduced hydration creating more space for further adsorption. The reflectivities of the same

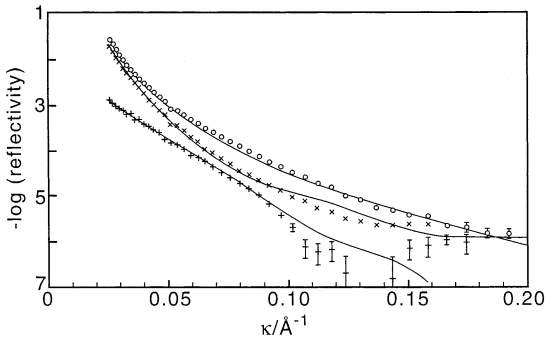

Figure 7. Neutron reflectivity profiles from the air/water surface of different isotopic compositions of 2.0×10^{-5} M $E_{23}P_{52}$ E_{23} at 35 °C. The observed profiles are shown as points, (○) dEhPdE in D_2O, (×) hEhPhE in D_2O and (+) dEhPdE in NRW. The best fits of a single structure to all three profiles, using the parameters in Table 4, are shown as continuous lines.

TABLE 4: Parameters for the Minimum Number of Layers Required to Fit the Interfacial Structure at Three Isotopic Compositions of 2.0×10^{-5} *M* $E_{23}P_{52}E_{23}$ in Water at 35 °C[a]

	concentration/*M*	2×10^{-5}
layer 1	τ_1/Å	9
	$10^6\rho$/Å^{-2}	0.3
	ϕ_{water}	0.0
layer 2	τ_2/Å	13
	$10^6\rho$/Å^{-2}	1.45
	ϕ_{water}	0.03
layer 3	τ_3/Å	5
	$10^6\rho$/Å^{-2}	5.0
	ϕ_{water}	0.59
layer 4	τ_4/Å	20
	$10^6\rho$/Å^{-2}	5.35
	ϕ_{water}	0.71
layer 5	τ_5/Å	25
	$10^6\rho$/Å^{-2}	6.4
	ϕ_{water}	0.91

[a] ρ denotes scattering length density and τ denotes layer thickness.

three isotopic compositions were measured at 35 °C at a copolymer concentration of 2.0×10^{-5} M. The effect of temperature is so large that at this concentration the coverage is actually greater than that at 1.2×10^{-3} M and 25 °C. The fitting procedure used was the same as described above and the reflectivity was fitted satisfactorily using a five layer model, as shown in Figure 7. Because only a four layer was necessary for this concentration at 25 °C, the structure of the layer has clearly changed with temperature. The fitted parameters are given in Table 4. The increased number of layers required for the model of the interface had no effect on the total monolayer thickness, but once again the thickness was found to be greater than the one obtained with a single uniform layer model. The area per molecule is reduced significantly from 430 Å^2 at 25 °C to 300 Å^2 at 35 °C. The increase of temperature therefore induces a considerable change in the monolayer structure, with increased overlap of the EO and PO distributions and a reduced hydration level within the monolayer.

The "smooth" volume fraction distribution at 35 °C is compared with that from the highest surface coverage at 25 °C in Figure 8. Although the two coverages are similar, there is a dramatic change in layer structure. The thickness of the upper layer above the surface, dominated by PO, doubles with the temperature increase and the extensive PO layer below the surface at 25 °C has collapsed. Interestingly, a proportion of EO segments have moved into the uppermost layer above the surface when the temperature increases to 35 °C without taking

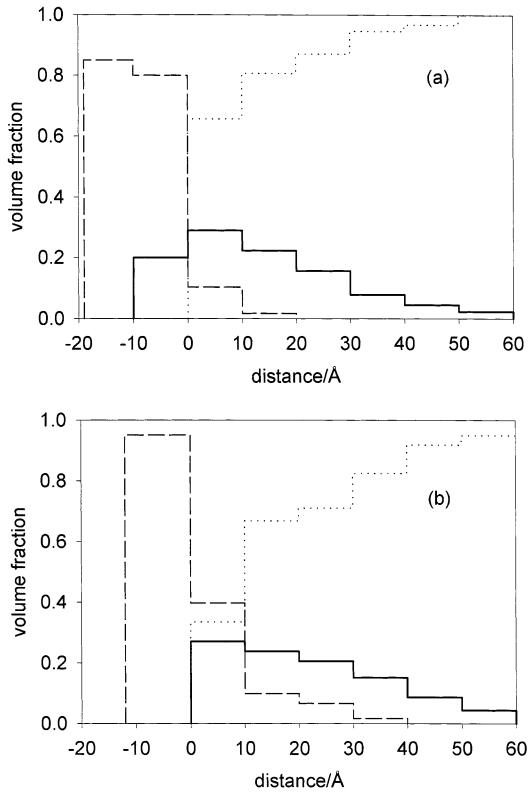

Figure 8. Volume fraction profiles of the three components PO (dashed line), EO (continuous line) and water (dotted line) at the air/water interface at (a) 35 °C and 2.0×10^{-5} M $E_{23}P_{52}E_{23}$ and (b) 25 °C and 1.2×10^{-3} *M* $E_{23}P_{52}E_{23}$.

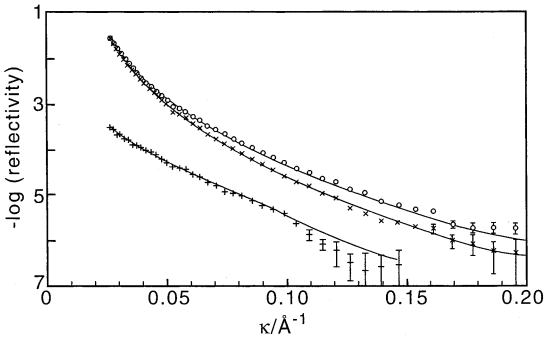

Figure 9. Neutron reflectivity profiles from the air/water surface of different isotopic compositions of 4.8×10^{-4} M $E_9P_{22}E_9$ at 25 °C. The observed profiles are shown as points, (○) dEhPdE in D_2O, (×) hEhPhE in D_2O and (+) dEhPdE in NRW. The best fits of a single structure to all three profiles, using the parameters in Table 5, are shown as continuous lines.

water with them. The general level of hydration of the layer is, as expected, greatly reduced.

Comparable measurements were also made on the much smaller molecular weight copolymer $E_9P_{22}E_9$. Two concentrations were studied, 4.8×10^{-4} M and 4.8×10^{-5} M, both within the region of the isotherm (section B) where there is a sudden increase in the surface excess. The three reflectivity profiles for each contrast at the two concentrations were adequately fitted with a four uniform layer model based on the monolayer structure that was applied to the $E_{23}P_{52}E_{23}$ data. Observed and calculated specular reflectivity profiles for the two concentrations are shown in Figures 9 and 10. The structural parameters are given in Table 5.

Similar comments can be made about the fitting as were made for the larger molecular weight copolymer. Thus, the parameters

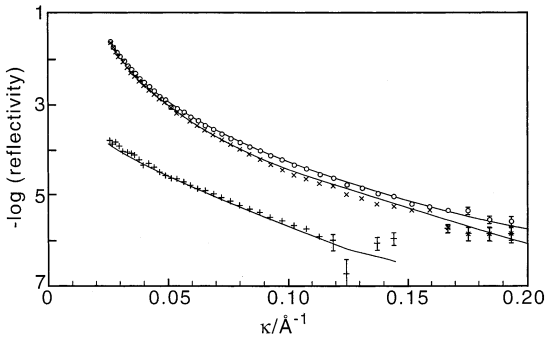

Figure 10. Neutron reflectivity profiles from the air/water surface of different isotopic compositions of 4.8×10^{-5} M $E_9P_{22}E_9$ at 25 °C. The observed profiles are shown as points, (○) dEhPdE in D_2O, (×) hEhPhE in D_2O and (+) dEhPdE in NRW. The best fits of a single structure to all three profiles, using the parameters in Table 5, are shown as continuous lines.

TABLE 5: Parameters for the Minimum Number of Layers Required to Fit the Interfacial Structure at Three Isotopic Compositions of $E_9P_{22}E_9$ in Water at 25 °C[a]

	concentration/*M*	4.8×10^{-4}	4.8×10^{-5}
layer 1	τ_1/Å	4	3
	$10^6\rho$/Å^{-2}	0.3	0.3
	ϕ_{water}	0.0	0.0
layer 2	τ_2/Å	13	8
	$10^6\rho$/Å^{-2}	1.90	1.63
	ϕ_{water}	0.58	0.60
layer 3	τ_3/Å	8	10
	$10^6\rho$/Å^{-2}	4.3	4.2
	ϕ_{water}	0.70	0.78
layer 4	τ_4/Å	25	25
	$10^6\rho$/Å^{-2}	6.4	6.4
	ϕ_{water}	0.93	0.95

[a] ρ denotes scattering length density and τ denotes layer thickness.

of the upper layer are not well determined and the total thickness of the four-layer monolayer model was thicker than that of the single layer model described in the previous paper. At 4.8×10^{-4} M, the four-layer monolayer thickness was 50 Å, whereas for the single-layer model, it was 45 Å. Once again, the clearest representation of the monolayer structure is in terms of a smoother distribution than used in the primary fitting and this is shown for the higher of the two concentrations in Figure 11. This plot immediately shows the much lower level of adsorption and the much greater degree of disorder in the layer in that there is more extensive overlap of PO and EO group distributions and of the PO groups even with water, quite unlike the structure of the larger copolymer. The greater interaction of PO with water is expected as the chain length decreases (short chain polypropylene glycols are actually soluble in water).

Discussion

On the face of it, a natural model to apply to the data would be the polymer brush, with the assumption that the insoluble PO block would act as a buoy for the soluble EO chains. If this were the case, the question would be whether the EO segment distribution would conform to a parabolic brush or a random coil, even though the EO chain lengths are strictly too short for such models to apply. Although the EO chains are short, it was nevertheless found that for the small molecule nonionic surfactants C_nE_m, where the EO chains are even shorter, the thickness of the EO chain region conforms rather well with random coil behavior.[4] Extrapolation from $C_{12}E_{12}$ would suggest that the width of the EO region for the present chain length should be 30−35 Å, rather shorter than observed. On the other hand, the fully extended length of the EO chains would be about 80 Å, only a little longer than observed. Although this might suggest that the brush model is more appropriate, the real difficulty of applying such a model to the EO chains is that the structure of the layer does not support the idea that the PO blocks are acting as anchors on the surface of the water. The significant fraction of PO penetrating the aqueous regions of the layer suggests that the ends of the PO block may act as part of the extended chain in the aqueous solution. The same feature is apparent in mean field calculations by Linse and Hatton.[5] These authors used an expanded mean field lattice theory to calculate the volume fraction profile across the air/water interface for an EPE copolymer. Our experimental volume fraction profile for $E_{23}P_{52}E_{23}$ shows a fair measure of agreement with their calculated volume fraction profile for $E_{37}P_{56}E_{37}$. Thus, the functional forms of the PO and EO profiles extending into the water subphase are similar for the experimental and theoretical distributions.The volume fraction estimated by the mean field model for EO groups close to the surface is, however, almost double the experimental value and the thickness estimated for the PO layer was slightly thinner, at 8 Å in comparison with the experimental value of 10−12 Å. The former may result from the greater number of EO groups in the polymer used for the mean field calculations and the latter may be because the experimental value of the thickness of the PO layer is the least certain of all the parameters and the experimental value will also have a contribution from capillary waves, which are not included in the mean field model.

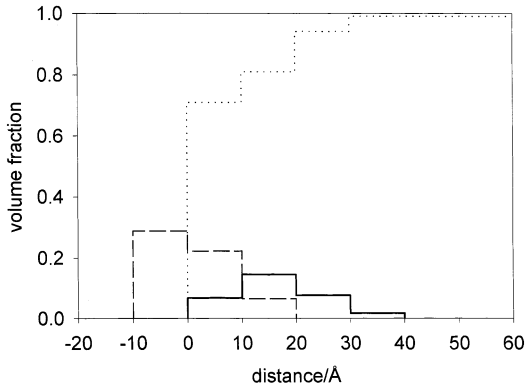

Figure 11. Volume fraction profiles of the three components PO (dashed line), EO (continuous line) and water (dotted line) at the air/water interface at 25 °C and 4.8×10^{-4} *M* $E_9P_{22}E_9$.

The nearest data available for comparison are neutron reflection data obtained for spread monolayers of copolymers of poly(butadiene) and ethylene oxide[6] and for soluble layers of copolymers of dimethylaminoethyl methacrylate and methyl methacrylate,[7] although neither could be regarded as at all close to the poloxamer system. Both systems form surface micelles. Because neutron reflection only determines the composition profile in the direction normal to the surface, it is not directly sensitive to the lateral structure generated by surface micelle formation. However, in both cases, the apparent mixing of the two fragments is extensive. The mixing of PO and EO observed in the present work is quite different. Relative to surface micelle formation the mixing in the poloxamer is much less extensive with the PO layer being much better defined than the corresponding hydrophobic fragment layers in the other two systems. The mixing of PO and EO therefore appears to be a genuine mixing in agreement with the mean field calculation of Linse & Hatton.[5] Although there are no other experimental structural data available for adsorbed poloxamer layers that could be used for comparison, several neutron small angle scattering studies

have been made of the micellar structure of the PEO−PPO−PEO triblock copolymers.[10−12] The first study by Mortensen and Pedersen did not attempt to define the internal structure of the micelle too closely but the unimer dimensions were determined and the aggregation was followed as a function of temperature. Goldmints et al., however, fitted four structural models of the micelle to their small angle scattering data.[11] In each of these, the PO and EO segments were regarded as completely segregated and the models differed in the amount of water included in the core (PO) and corona (EO) regions. Their final conclusion was that for the commercial P85 (nominally $E_{25}P_{40}E_{25}$) the core consisted of 60% water and 40% PO at 31.4 °C and the micellar radius was in the range 50−64 Å, to be compared with values of 71−90 and 80 Å from NMR and dynamic light scattering, respectively. In this work, the EO and PO were both in their fully hydrogenated forms and they are then more or less indistinguishable. However, in a more recent study by Goldmints et al., the triblock studied consisted of hydrogenated PO and deuterated EO, just as in the present reflection study. Goldmints et al. studied the micelle structure at temperatures from 41 °C up to 49 °C, and this enabled them to reduce the micellar concentration to a level where they could justifiably neglect any contribution from the interparticle scattering. The final model Goldmints et al. fitted was consistent with the earlier analysis giving, at 41 °C, a core consisting of 37% PO by volume and 63% water with a corona of 11% EO and 89% water. Although they obtained excellent fits to their data, the model used by Goldmints et al. has a fragment and water distribution that is not at all like what we have observed at the air/water interface. There are two crucial differences. First, in the adsorbed layer, the most hydrophobic region, the PO part of the layer, contains no water at all, whereas the micellar core contains a large fraction of water. Second, the adsorbed layer separates the pure PO region from the aqueous/EO tail region by a mixed layer of PO, EO, and water, which is of a thickness comparable to the PO only layer. At the temperature used in the studies by Goldmints et al., this layer is particularly pronounced and contains less water. Because both micellar aggregation and adsorption at the air/water interface are both driven by the hydrophobic effect, it seems unlikely that the effects of curvature in the micelle could lead to such fundamental differences between the two structures. It is also interesting to note that the micellar structure of Goldmints et al. is in conflict with an earlier paper from the same group, which used a fluorescence probe to determine the composition of the micellar core and concluded that for P105 (nominal stoichiometry $E_{37}P_{56}E_{37}$) the core consisted of 72% PO, 28% EO, and no water.[13] No doubt the reasons for overriding the earlier results were that neutron small angle scattering should give an unambiguous structure for micelles of this sort of size. However, as we shall now show, the Pluronic structures may be unusual in this respect.

The comparison of the structure of a flat layer at the air/water interface with the structure of a micelle should be undertaken with caution. Helpful correlations between the two may be made for small surfactant molecules, e.g.,[8] especially given that neutron reflection has a significant resolution advantage (for a discussion of the resolution in reflection experiments see ref 9). For molecules as large as the present EO−PO−EO copolymers the radial geometry of the micelle may have a large influence on the distribution of the PO and EO groups. Nevertheless, one would expect a little more resemblance than that outlined in the previous paragraph. We have therefore atempted to recalculate the small-angle scattering patterns using fragment distributions that are qualitatively closer to those we have observed at the flat surface. Because we needed a minimum of four layers to describe the layer at the air/water surface we start by assuming that four layers may be the minimum number of layers needed to represent the micellar structure adequately. On the basis of the surface layer, we would expect the micellar core to be very much dominated by PO, followed by a region containing significant amounts of EO mixed with PO, and then two EO layers with only small amounts of PO in each. We only attempted to fit one complete set of small angle scattering data and that was the data obtained by Goldmints et al. at 41 °C. With the four shell structure we have just described we were surprised to find as acceptable a fit as the original fit of Goldmints et al., but with a structure qualitatively more in line with the structure of the adsorbed layer (note that the reverse calculation, i.e., using the micellar model to calculate the neutron reflection data, does not work even approximately). The calculated profiles for our structure are superimposed on their *calculated* profiles in Figure 12 and the excellent agreement of the two alternative models of the micelle is clear (the reason for choosing their calculated structure was that it is more accessible and their model fits seemed to be in excellent agreement with their experimental data). The two structures are compared in Table 5. The only obvious similarity between them is that the aggregation numbers agree closely.

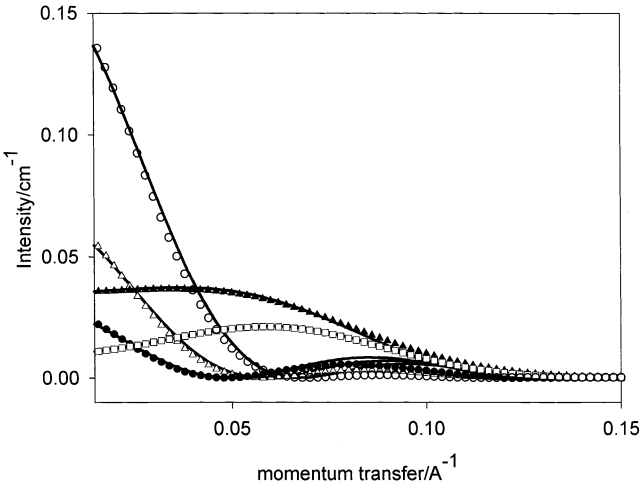

Figure 12. Comparison of small angle scattering patterns calculated for a model of the micelle based on the structure of the adsorbed layer of $E_{23}P_{52}E_{23}$ at the air/water interface compared with the calculated profiles used to fit a core−shell model of $dE_{23}hP_{34}dE_{23}$ at 41 °C by Goldmints et al. (ref 12), for which the parameters are given in Table 6. Lines are the scattering patterns from the core/shell model and points are calculated using the data also given in Table 6. The contrasts are (○) 14% D_2O, (△) 30% D_2O, (●) 40% D_2O, (□) 70% D_2O, and (▲) 80% D_2O.

TABLE 6: Best Fit of a Four-Shell Model to Small-Angle Scattering Data at 41 °C

	radius /Å±1	volume fractions ±0.01			no. of units per polymer in micelle		
		ϕ_{PO}	ϕ_{EO}	ϕ_{water}	n_{PO} /N±0.5	n_{EO} /N±0.5	n_{water} /N±5
shell1	14	0.80	0.06	0.14	4.5	0.5	2.5
shell 2	28	0.51	0.057	0.433	20.0	3.5	55
shell 3	40	0.055	0.055	0.89	4.5	7.0	240
shell 4	66	0.01	0.05	0.94	4.5	35.0	1360
core[a]	35.4±	0.37	0	0.63	34	0	185
corona[a]	56±	0	0.11	0.89	0	46	780

N is the aggregation number of the micelle and is equal to 21. [a] Model used by Goldmints et al.[12]

The part of our structure that could be regarded as approximately equivalent to the core of the model of Goldmints et al. consists of a core of 14 Å radius containing 80 vol % PO, 6% EO, and 14% water, and a second shell of thickness 14 Å (radius 28 Å) containing much less PO (51 vol %), 5.7% EO, and 43.3% water. Our third shell has a thickness of 12 Å (radius 40 Å) and contains 5.5% PO, 5.5% EO, and 89% water, and there is even some PO in the outer shell. Although the latter is only 1% the effect of radial integration is that it represents a significant amount of PO. Averaging over the central part of this distribution out to the core radius of 35.4 Å used by Goldmints et al. gives a mean volume fraction of 29.5% PO, 65% water, and 5.5% EO, which is not too different from their values of 37% PO and 63% water. This is presumably the reason that the set of small angle scattering contrasts are well fitted by the two different structures. Despite this low resolution similarity, our proposed structure for the micelle is qualitatively quite different. Furthermore, it bears a physically reasonable resemblance to the structure at the air/water interface, and it is consistent with the earlier fluorescence probe measurements of Goldmints et al. It might be argued that a change in structure, such as that we have observed in the adsorbed layer between 25 °C and 35 °C, will occur in the micelle on heating to 41 °C, which was the temperature of the observations of Goldmints et al. This is possible but the change in the structure that occurs on heating the layer to 35 °C seems to be even less compatible with that proposed by Goldmints et al.

The discrepancy between the two models that both fit the small-angle scattering data has some worrying implications for the interpretation of small-angle scattering in more complex systems. Goldmints et al. followed the standard practice of using the minimum number of shells (layers) required to fit the data. In that we have used four shells to fit the data when only two are necessary means that we have introduced a model which has a higher resolution than may be appropriate for SANS data. This does not mean that our structure of the micelle is correct; there may be better ones which will not be established until the small-angle scattering has been studied over a wider range of contrasts and conditions. However, neither the feature of no PEO/PPO mixing nor the high PO core water content in the Goldmints et al. micellar structure accord well with the observation that aqueous PPO/PEO mixtures (albeit with rather small molecular weights) are miscible over a large part of the composition range.[14]

Acknowledgment. We thank Dow AgroSciences for financial support and we are also grateful for financial support from the Engineering and Physical Science Research Council of the United Kingdom.

References and Notes

(1) Alexandridis, P.; Athanassiou, V.; Fukuda, S.; Hatton, T. A. *Langmuir* **1994**, *10*, 2604.
(2) Vieira, J. B.; Li, Z. X.; Thomas, R. K. *J. Phys. Chem.* Submitted.
(3) Penfold, J.; Richardson, R. M.; Zarbakhsh, A.; Webster, J. R. P.; Bucknall, D. G.; Rennie, A. R.; Jones, R. A. L.; Cosgrove, T.; Thomas, R. K.; Higgins, J. S.; Fletcher, P. D. I.; Dickinson, E.; Roser, S. J.; McLure, I. A.; Hillman, R. A.; Richards, R. W.; Staples, E. J.; Burgess, A. N.; Simister, E. A.; White, J. W. *J. Chem. Soc. Far. Trans.* **1997**, *93*, 3899.
(4) Lu, J. R.; Su, T. J.; Li, Z. X.; Thomas, R. K.; Staples, E. J.; Tucker, I.; Penfold, J. *J. Phys. Chem.* **1997**, *101*, 10 339.
(5) Linse, P.; Hatton, T. A. *Langmuir* **1997**, *13*, 4066.
(6) Bowers, J.; Zarbakhsh, A.; Webster, J. R. P.; Hutchings, L. R.; Richards, R. W. *Langmuir* **2001**, *17*, 131.
(7) An, S. W.; Thomas, R. K.; Baines, F. L.; Armes, S. P.; Billingham, N. C.; Penfold, J. *J. Phys. Chem. B* **1998**, *102*, 5120.
(8) Jackson, A. J.; Li, Z. X.; Thomas, R. K.; Penfold, J. *Phys. Chem. Chem. Phys.* **2002**, *4*, 3022.
(9) Li, Z. X.; Thirtle, P. N.; Weller, A. T.; Thomas, R. K.; Penfold, J.; Webster, J. R. P.; Rennie, A. R., *Proc. 5th Int. Conf. Surface X-ray & Neutron Scattering*; Norman, D., Webster, J. R. P., Eds.; North-Holland, 1998, 171.
(10) Mortensen, K.; Pedersen, J. S. *Macromolecules* **1993**, *26*, 805.
(11) Goldmints, I.; von Gottberg, F. K.; Smith, K. A.; Hatton, T. A. *Langmuir* **1997**, *13*, 3659.
(12) Goldmints, I.; Yu, G. A.; Booth, C.; Smith, K. A.; Hatton, T. A. *Langmuir* **1999**, *15*, 1651.
(13) Nivaggioli, T.; Alexandridis, P.; Hatton, T. A.; Yekta, A.; Winnik, M. A. *Langmuir* **1995**, *11*, 730.
(14) Malmsten, M.; Line, P.; Zhang, K. W. *Macromolecules* **1993**, *26*, 2905.